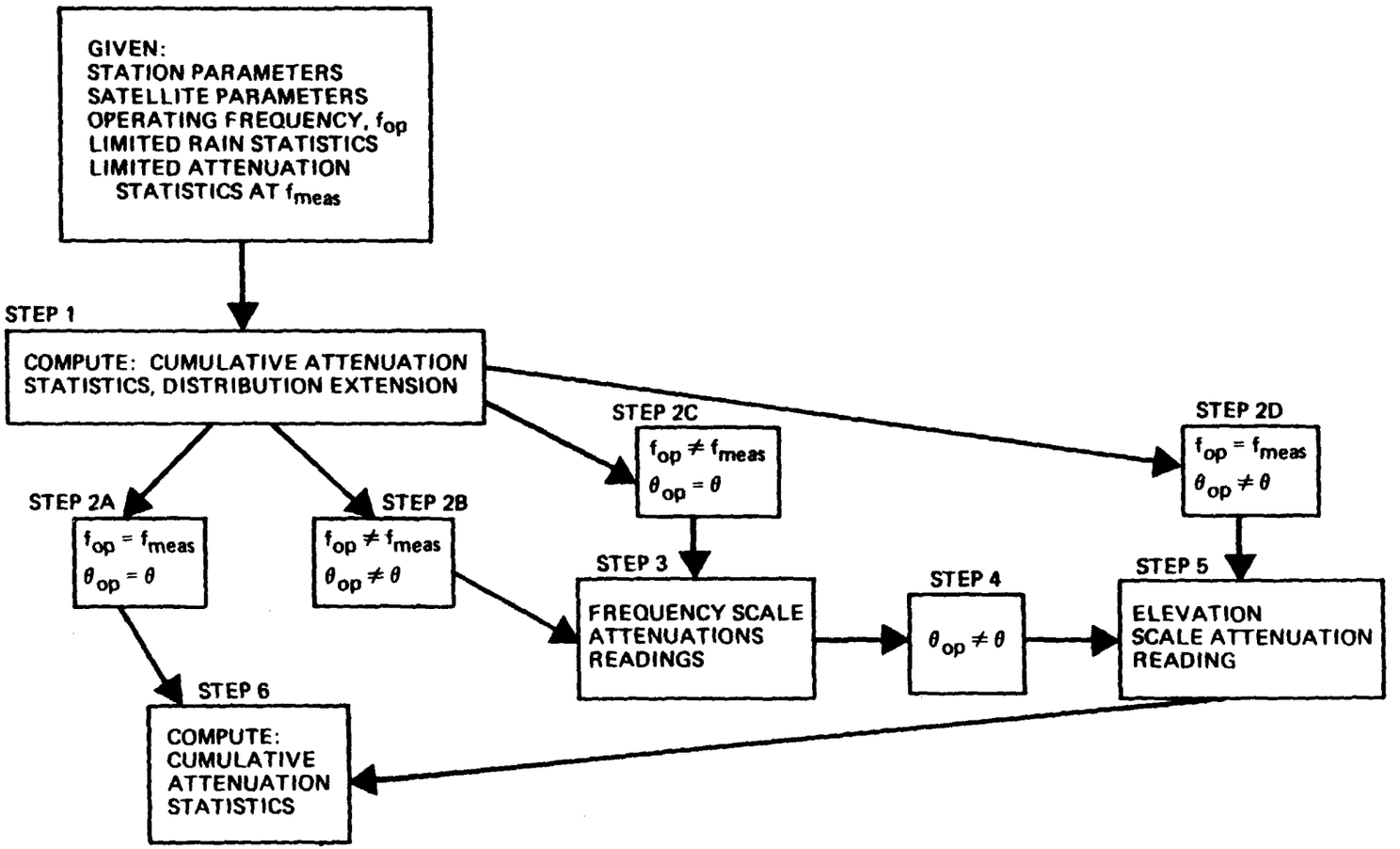

Figure 6.3-10. Procedure for Generation of Cumulative Attenuation Statistics Given Limited Rain Rate and Attenuation Statistics

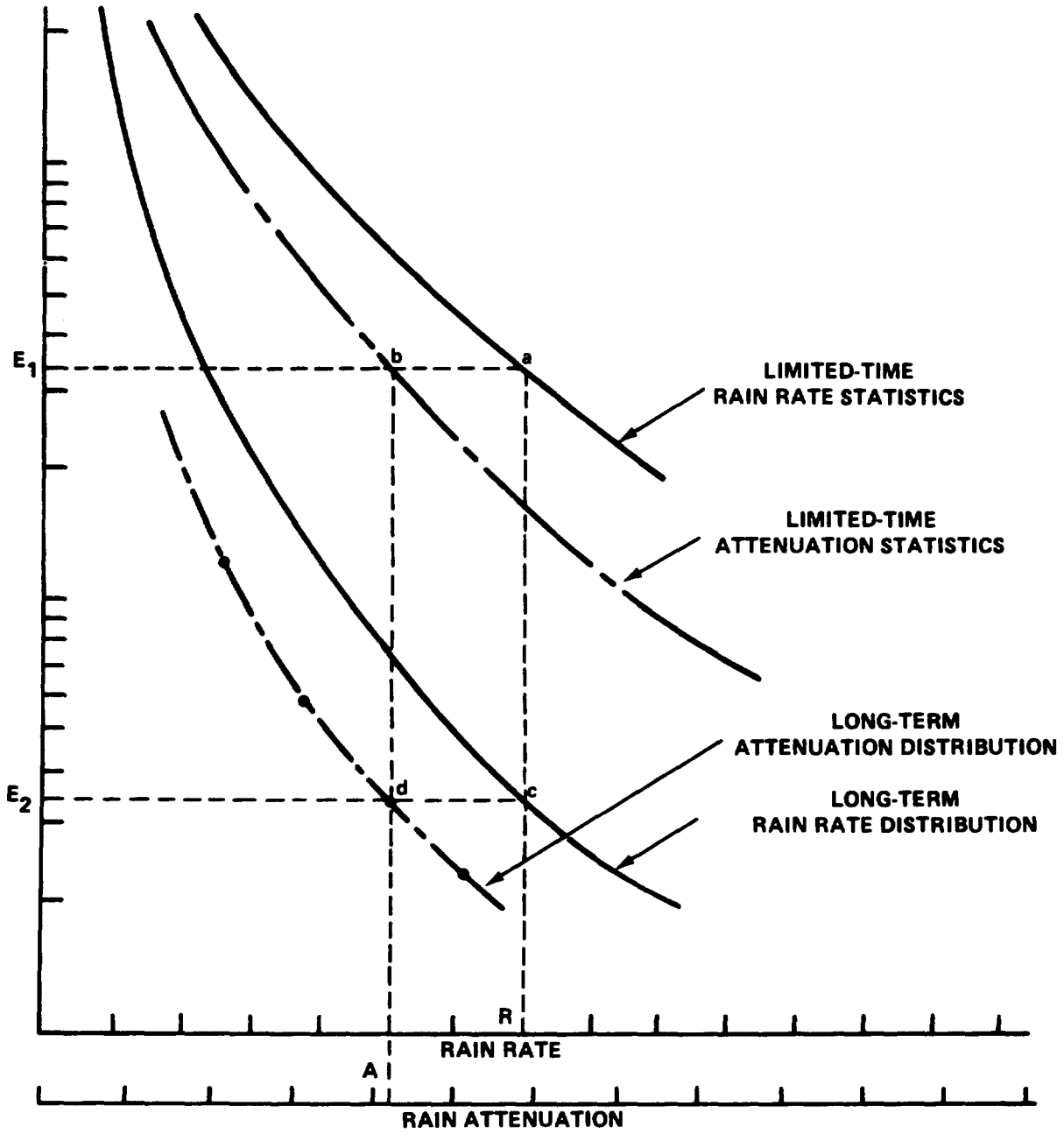

Figure 6.3-11. Construction of Cumulative Attenuation Statistics Using the Distribution Extension Technique

4. Repeat the process for several points and join them with a smooth curve.

Distribution extension in this manner assumes that the values of rain rate and attenuation remain the same as the measured values, on the average, for times of the year different than the measurement period. This is not necessarily so. The physical distribution of raindrops along the propagation path in a stratiform rain, for example, differs from the distribution in a mild convective storm. Both conditions could produce local rainfall at the same rate, but the attenuation produced could be quite different. Thus in regions where there is wide seasonal variation in how rain falls, distribution extension should be used with caution. The reliability of the extended distribution depends on how "typical" of the whole year the rainfall was during the measurement period. If the shapes of the limited-time and the long-term distribution curves are similar, the limited-time sample is statistically significant and the distribution extension will be valid.

6.3.4.3 Frequency Scaling. If frequency scaling of measured rain attenuation (Step 3 of Figure 6.3-10) is required, the specific attenuation scaling technique is recommended. In this technique specific attenuation data is utilized to scale the attenuation A from frequency f_1 to frequency f_2. Referring to the equation for rain attenuation in Step 7 of Figure 6.3-1, the result is

$$\frac{A_2}{A_1} = \frac{k_2}{k_1} R_p^{\alpha_2 - \alpha_1} \cong \frac{k_2}{k_1} \quad (\text{for } \alpha_1 \cong \alpha_2) \qquad (6.3\text{-}17)$$

where

$$A_1 = A_1(f_1), \quad A_2 = A_2(f_2), \quad k_1 = k_1(f_1), \ . \ . \ . \ , \text{ etc.} \qquad (6.3\text{-}18)$$

This is a fair estimate for small frequency ratios (e.g., less than 1.5:1), and moderate rain rates, but errors can be large otherwise. This is because the above equation implicity assumes that rainfall

is homogeneous over the propagation path, which is usually not true. By assuming a simple Gaussian model for the rain rate with distance along the path, Hodge (1977) derived an expression for attenuation ratio that includes an inhomogeneity correction factor, and uses the high correlation between attenuation and peak rain rate to eliminate the rain rate:

$$\frac{A_2}{A_1} = \frac{k_2}{k_1}\left(\frac{A_1\sqrt{\frac{\alpha_1}{\pi}}}{k_1}\right)^{\frac{\alpha_2}{\alpha_1}-1}\sqrt{\frac{\alpha_1}{\alpha_2}} \qquad (6.3\text{-}19)$$

This yields a better fit to empirical data.

6.3.4.4 Elevation Angle Scaling. Step 5, the elevation angle scaling between the operational elevation angle θ_{op} and the measured data angle θ_{meas} is somewhat complex. The first order approximation, the cosecant rule, is recommended, namely

$$\frac{A(\theta_2)}{A(\theta_1)} = \frac{\csc\,\theta_2}{\csc\,\theta_1} = \frac{\sin\,\theta_1}{\sin\,\theta_2} \qquad (6.3\text{-}20)$$

If more detailed calculations are desired the full formulas in Figure 6.3-1 are utilized.

6.3.4.5 Example of Distribution Extension. Figure 6.3-12 shows an example of applying the distribution extension technique. The upper two curves are cumulative rain-rate and attenuation statistics derived from more than 600 total minutes of measurements over the July through December 1974 period. The bottom curve in the figure is the measured distribution of rain rate for the entire six-month period (263,000 minutes). Comparison of the two rain rate distributions shows that they are very similar in shape. This indicates that the rain rate measurements made during attenuation measurements are a statistically significant sample of the total rainfall, and that using the distribution extension technique is

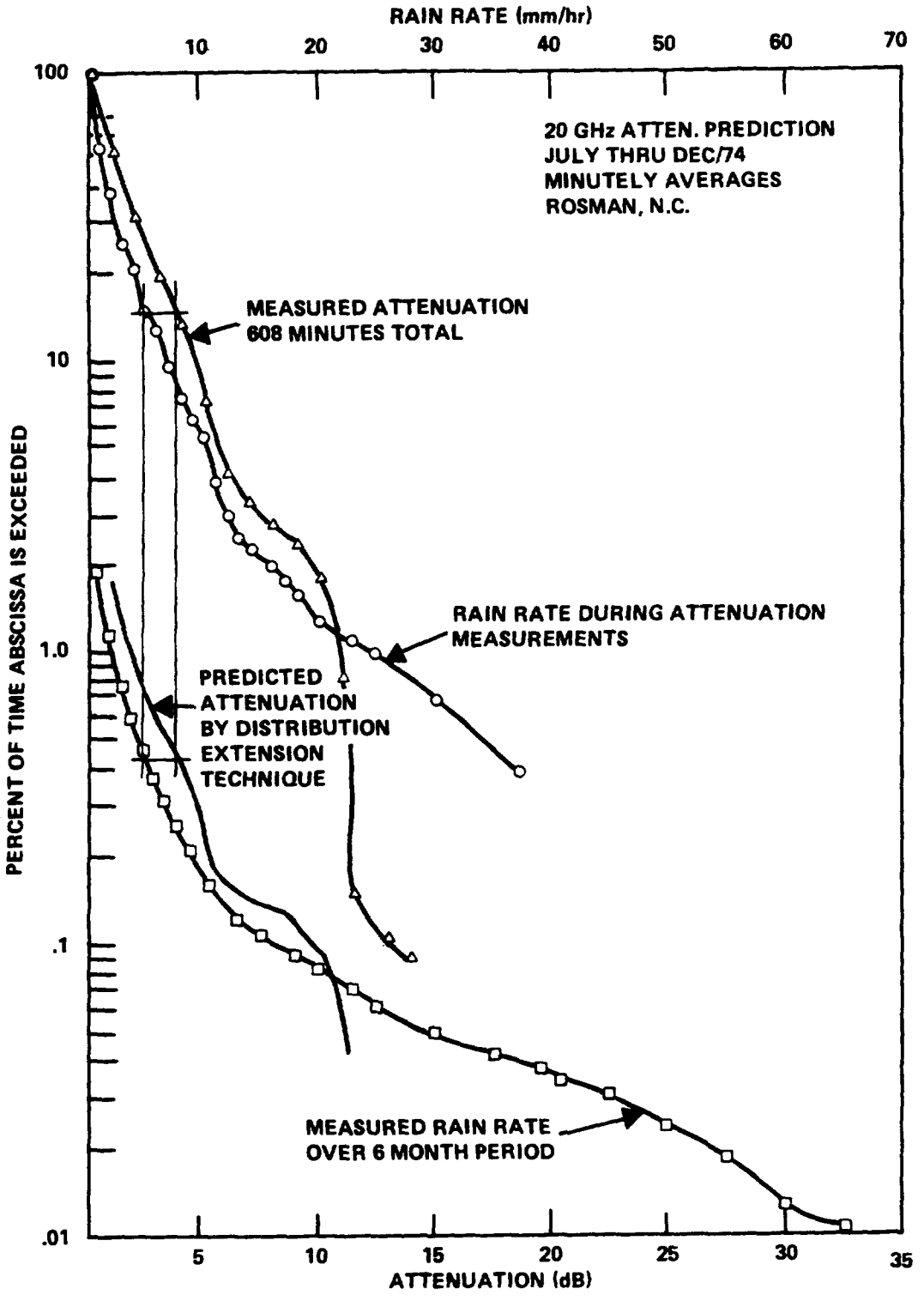

Figure 6.3-12. Example of Distribution Extension Technique

valid. The extended attenuation distribution, constructed as described in paragraph 6.3.4.2, is shown in the figure.

6.3.5 Fading Duration

System designers recognize that at some level of rain rate R_m the entire system margin will be utilized. The cumulative rain rate statistics indicate the percentage of time the rain rate exceeds R_m. In this section, a technique is presented for estimating an upper bound on the duration of the periods that the rain rate exceeds a given R_m. This is equivalent to the duration of fades exceeding the depth corresponding to R_m.

Experimental fade duration statistics are presented in Chapter 5 (Section 5.6). As mentioned in that section, experimental data has confirmed that the duration of a fade greater than a given threshold tends to have a log-normal probability distribution. This is equivalent to the logarithm of the duration having a normal distribution. Given sufficient experimental data, one may determine the parameters of the best-fitting log-normal distribution, and use these to extrapolate from the empirical distribution. Such extrapolation could be used in lieu of, or in addition to, the technique described here when fade duration data is available.

6.3.5.1 Estimating Fade Duration Versus Frequency of Occurrence. The US and Canadian weather services have published maximum rainfall intensity (rain rate) - duration - frequency curves which provide the point rain rates for several hundred locations on the North American continent (U.S. Dept. Comm.-1955 and Canada Atmos. Env.-1973). Two typical sets of curves for the close-proximity cities of Baltimore, MD and Washington, D.C. are shown in Figure 6.3-13. The return periods are computed using the analysis of Gumbel (1958) since data is not always available for the 100-year return period. These curves are derived from the single maximum rain-rate event in a given year and are termed the annual series. For microwave propagation studies, curves that consider all high rain rate events are necessary. Such curves, called the partial-duration series, are

not normally available, but empirical multipliers have been found for adjusting the annual series curves to approximate the partial-duration series (Dept. Commerce-1955). To obtain the partial-duration curve, the rain rates on the annual series curve for the desired return period are multiplied by the appropriate factors, given in Table 6.3-4.

Table 6.3-4. Multiplicative Factors to Convert Annual to Partial-Duration Series

RETURN PERIOD (YEARS)	MULTIPLY ANNUAL SERIES RAIN RATE BY
2	1.13
5	1.04
10	1.01
25, 50, 100	1.00

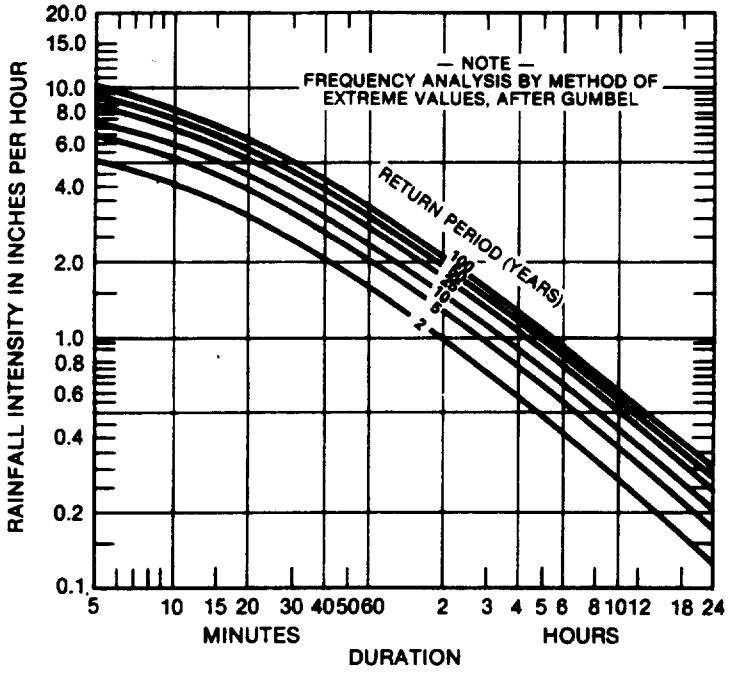

WASHINGTON, D.C.
1896—1897, 1899—1953

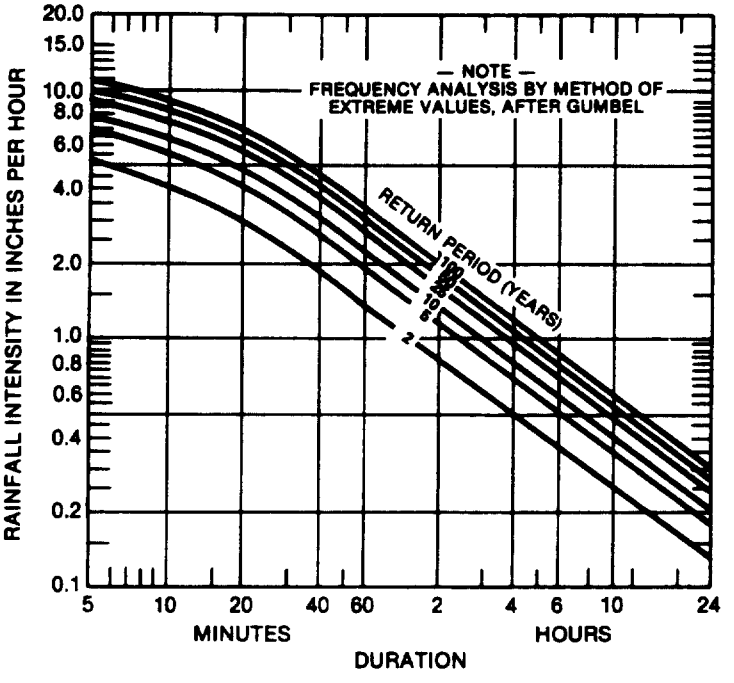

BALTIMORE, MARYLAND
1903—1951

Figure 6.3-13. Typical Rain Rate-Duration-Frequency Curves From U. S. Weather Service, Annual Series

The intensity-duration-frequency curves actually give the average rain rate over the duration period, whereas the instantaneous rain rate is of interest from a propagation standpoint. The curves therefore do not directly give the frequency versus duration of fades of a given depth. However, for short averaging periods (e.g., five minutes), the instantaneous rain rate would be expected to stay fairly close to the average rain rate, and would certainly never exceed it for the entire period. The curves then can be used to approximate the frequency of short-duration fades, and to place an upper bound on the frequency in any case.

The minimum return period shown on Figure 6.3-13 is two years. It is desirable to be able to extrapolate to one year. This can be done using the Gumbel frequency analysis technique for extreme values. This has been accomplished graphically, for durations of 5 through 60 minutes as shown in Figure 6.3-14. The data used in the curves has been adjusted using the multipliers of Table 6.3-4 to correspond to the partial-duration series. For example, the rain rate expected in Baltimore in a 5-minute period once in 2 years is 5.2 x 1.13 = 5.9 inches per hour. Extrapolating to one year yields 4.8 inches per hour (122 mm/h). Similar calculations may be done for other duration periods to generate a 1-year return period curve for the partial-duration series.

The recommended technique for estimating the maximum fade period to be expected in an N-year rain event is described in Figure 6.3-15. Here the station parameters (latitude, longitude, etc.), operating frequency and link margin (after clear air attenuation is removed) are required inputs. By iteratively solving the attenuation equation in Figure 6.3-1 the maximum allowable point rain rate R_{pm} is obtained. The estimate of the maximum fade duration for the worst rain in 1,2,5,10 or more years is then obtained from data for the partial-duration series rain rate-duration-frequency curves (see Figure 6.3-9). For example, if the system maximum allowable rain rate R_{pm} is 5 inches/hour (125 mm/hr), a system in

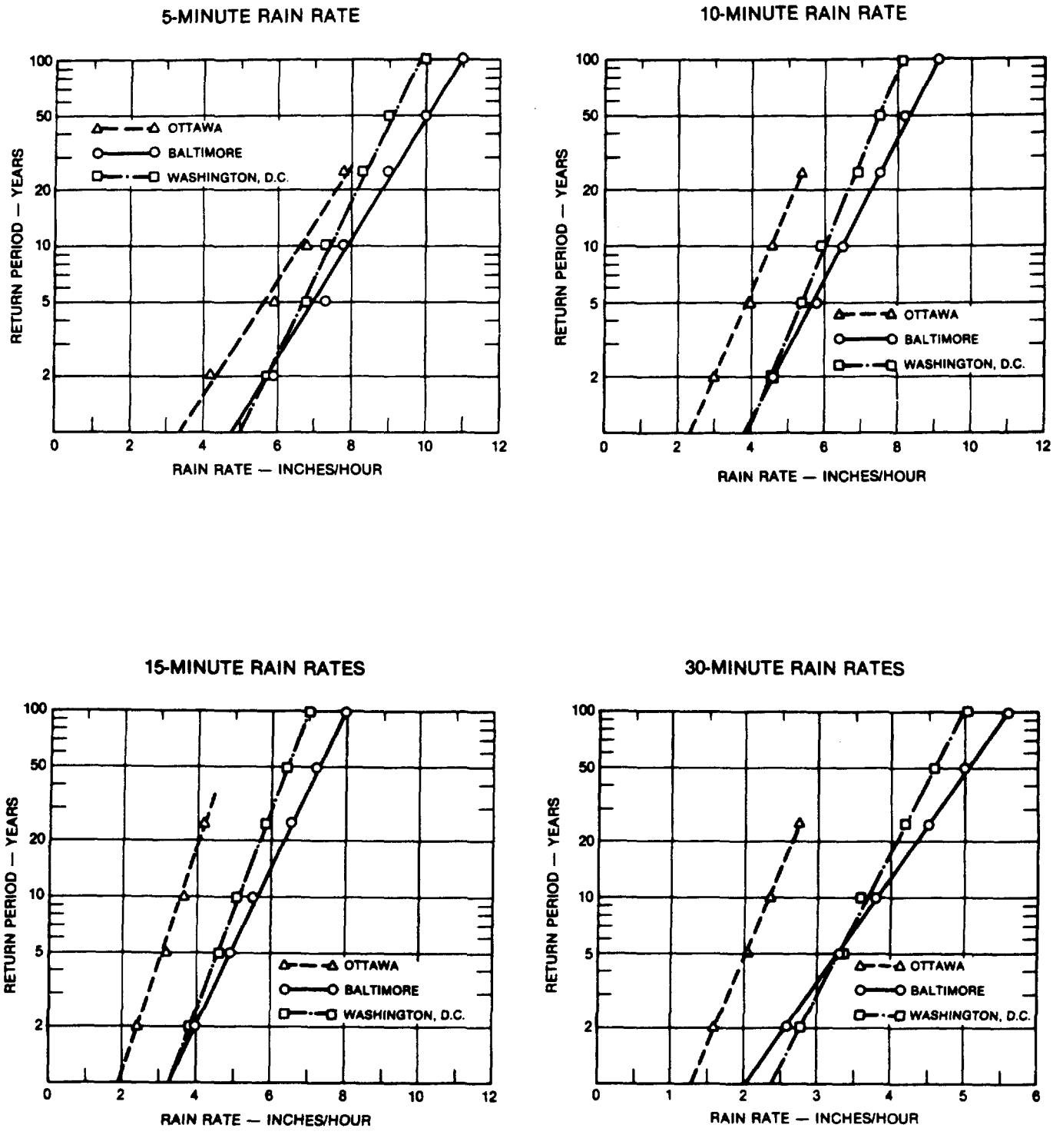

Figure 6.3-14. Extrapolated Partial-Duration Rain Rate-Duration-Frequency Curves

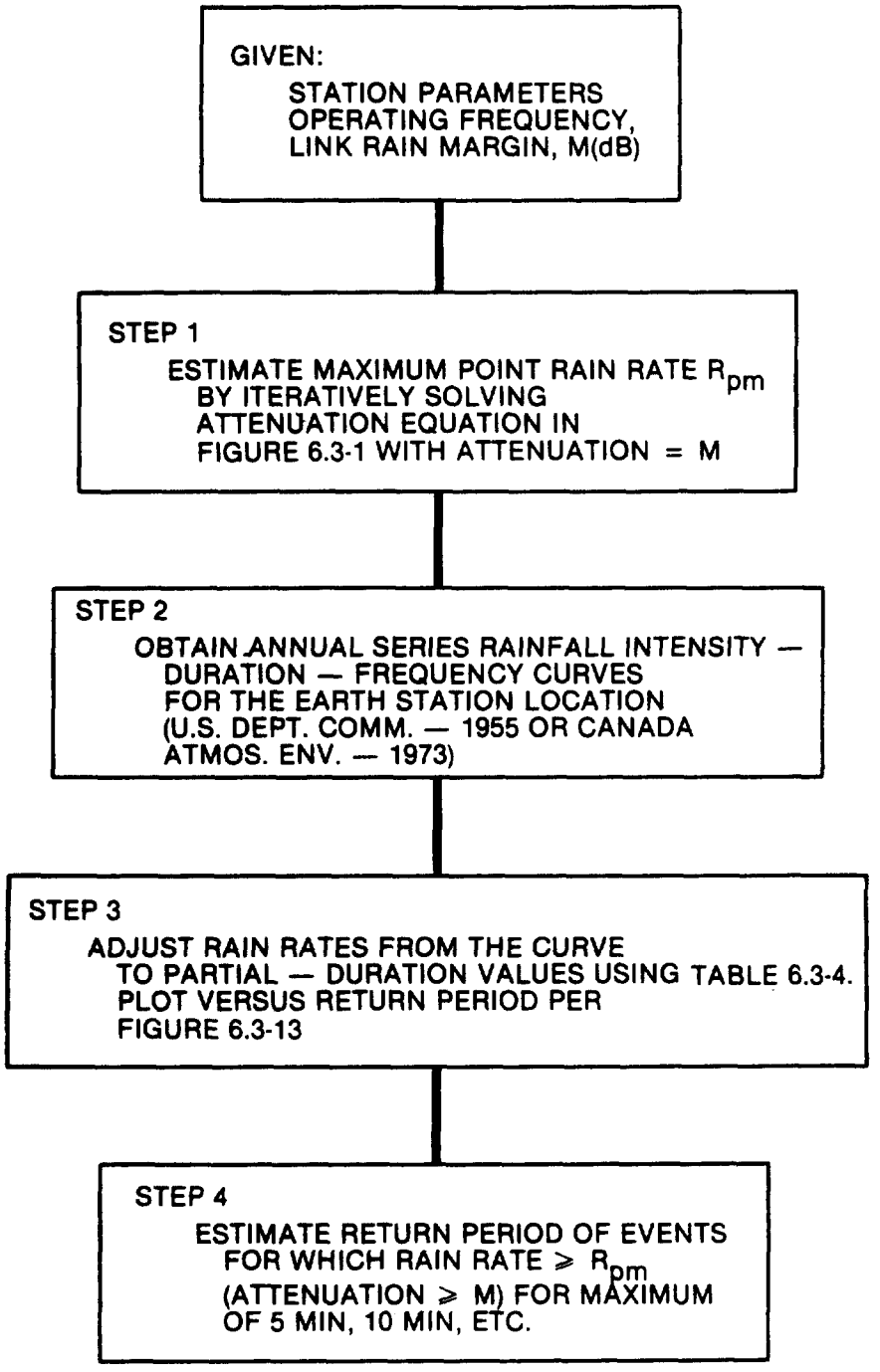

Figure 6.3-15. Technique for Estimating Frequency of Occurrence of Fades of Given Duration

Washington, D.C. should on the average expect one maximum 5-minute fade each year, one maximum 10-minute fade every three years, etc.

6.3.5.2 Annual and Daily Temporal Distribution of Intense Rain Events. The temporal distribution of rain-induced fade events can be important to a designer since loss of a link during low utilization periods may be tolerable. Figure 6.3-16a shows the distribution, by season, of "record" rainfall events at 207 weather stations throughout the U.S. The events are measured in terms of depth-duration, which specifies the total number of inches of rain and the time over which it fell. The durations are shown in the figure, and range from 5 minutes to 24 hours. Figure 6.3-16b shows the distribution of the maximum events by the times when they start. It is clear that the short-duration events, having the most intense rain (and the deepest fades) occur predominantly in the summer months and during the afternoon hours. There are regional variations, of course: throughout much of the west coast, summer rains are insignificant. In the midwest, nocturnal thunderstorms are common. The figure also shows that more than 40% of the record 24-hour rainfall events happen in the fall, when steady stratiform rains are the rule. The regional variations in the time distribution of heavy rains is clearly shown in Figure 6.3-17 (Rasmusson- 1971). It gives the time of day of the maximum thunderstorm frequency, based on 10 years' observations. A phenomenon not indicated by the map is the existence of secondary peaks in thunderstorm frequency in many regions.

6.3.6 Rate of Change of Attenuation

Experimental data related to the rate-of-change of attenuation is relatively sparse. Apparently experimenters have not analyzed their measurements to obtain this information except during some extreme attenuation occurrences. Some measurements made at Rosman, NC of the CTS 11.7 GHz beacon showed a maximum rate-of-change of 2 dB/sec on April 24, 1977 (Ippolito-1979). This translates to change of rain rate from 50 mm/hr to 57 mm/hr in one second. Assuming this

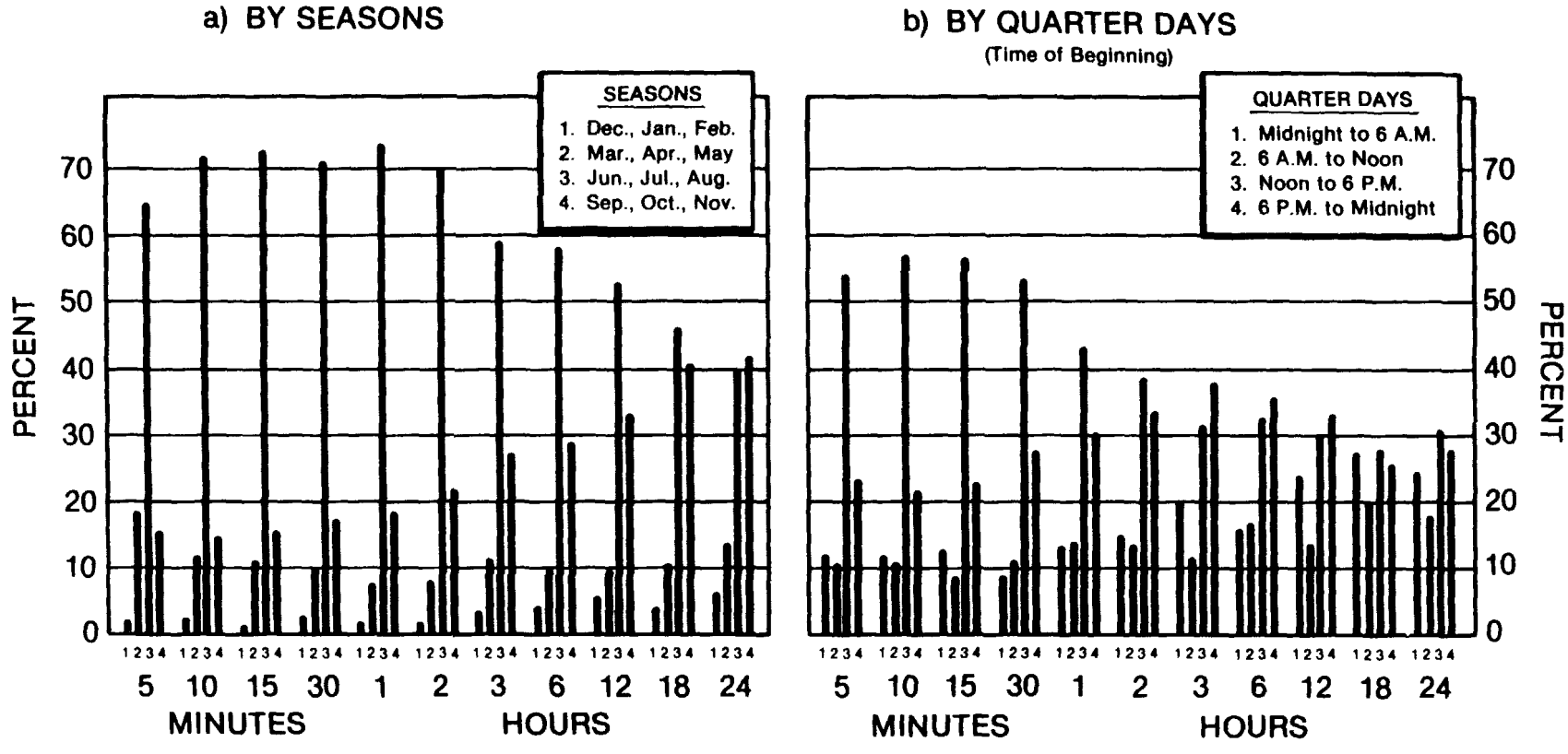

Figure 6.3-16. Distribution of Maximum Rainfall Occurrences at U.S. First-Order Stations (U.S. Dept. Comm.-1947)

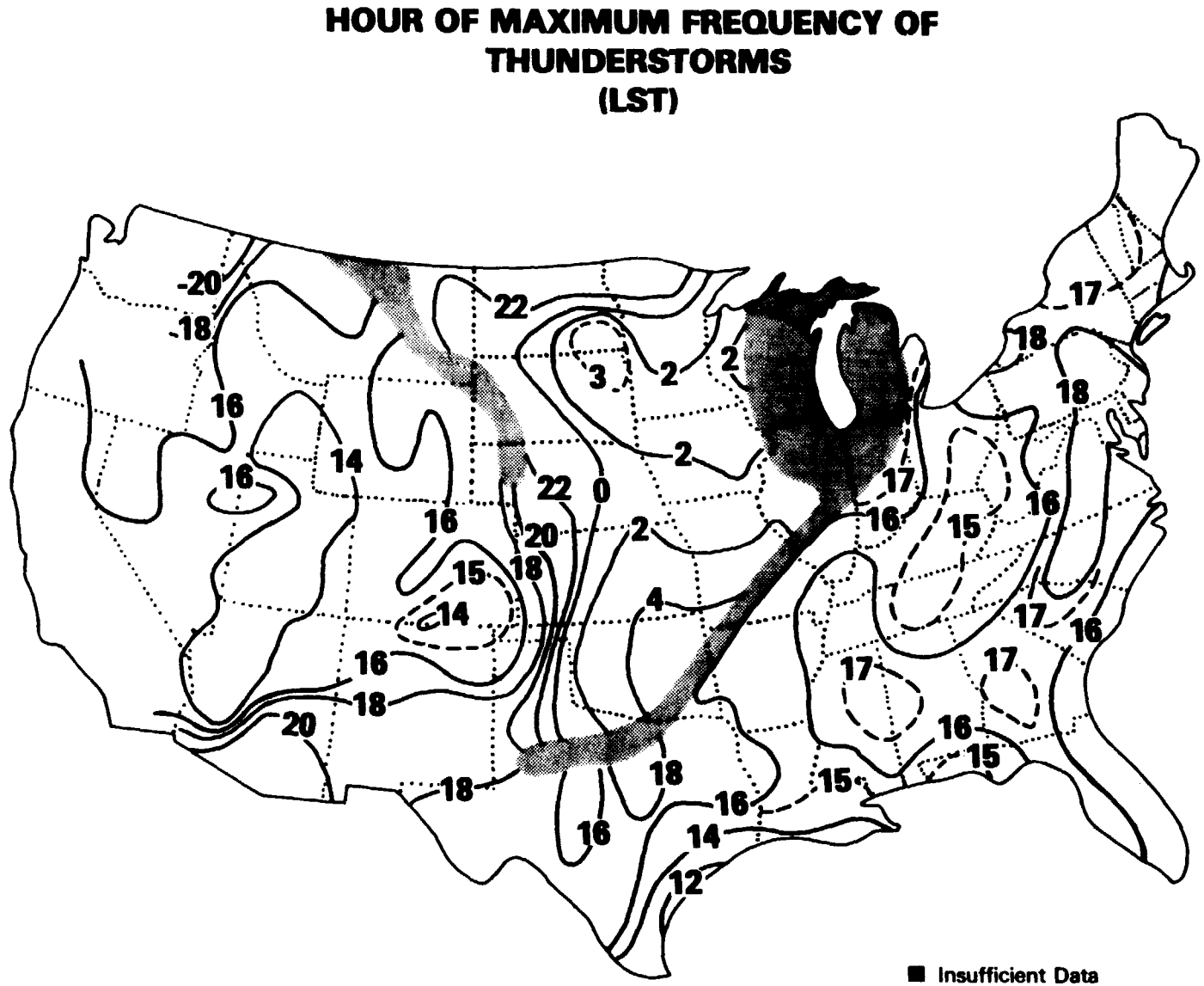

Figure 6.3-17. Time of Day When Maximum Thunderstorm Frequency Occurs (Rasmusson - 1971)

change in rain rate, the rate of change of attenuation would have been 4 dB/sec at 20 GHz.

Maximum fade rates of 0.1 dB/sec at 15 GHz are reported by Hodge (1974) and Strickland (1977). Dintelmann (1981) reports fade rates of up to 0.6 dB/sec in Europe at 11.7 GHz.

6.3.7 Worst-Month Statistics

Worst-month statistics are of interest to those faced with designing a system to meet performance criteria expressed in terms of a percentage of any calendar month, or of any contiguous 30-day period. The system designer in this case needs to find the percentage of time that some threshold value of attenuation or rain rate will be exceeded within a given month. For every threshold value, there corresponds a month of the year having the highest percentage of time exceeding the threshold (i.e., the percentage exceedance). This is designated the "worst-month" for that threshold. The percentage exceedance in this month, to be expected once every year or every given number of years, is of most interest. For high rain rates, the worst-month would probably correspond to the period of highest thunderstorm intensity or frequency, whereas the worst-month for lower rain rates might be when most rainfall is of the steady, stratiform variety.

An exponential model has been devised (Crane and Debrunner-1978 and CCIR-1978, Rpt 723) for estimating the ratio of the percentage exceedance for a given threshold value in the worst-month to the average annual percentage exceedance for the same threshold. This exponential relationship is expected for statistics of rare events (Gumbel-1958).

Let X_{ij} be the percentage exceedance in month i corresponding to a threshold rain rate j. In a given year, there is for each value j a month h with the highest X_{ij}, denoted X_{hj}. The worst-month statistic is the value of X_{hj} that is equalled or exceeded, on average, once in N years where N (the return period) is specified.

The probability that the worst month percentage exceedance is equal to or greater than X_{hj} is given by:

$$P(X_{hj}) = \frac{1}{12N} \tag{6.3-21}$$

The exponential model, which applies when X_{hj} is small, states:

$$P(X_{hj}) = C_{oj} \exp(-X_{hj}/C_{1j}) \tag{6.3-22}$$

where C_{oj} and C_{ij} are empirical constants. Inverting this equation yields:

$$X_{hj} = C_{1j} \ln C_{oj} - \ln P(X_{hj}) \tag{6.3-23}$$

Figure 6.3-18 is a plot of monthly probabilities of exceeding preselected thresholds X_{ij} for 44 consecutive months of attenuation measurements. It clearly follows the straight-line relation of the model, with $C_{oj} = 0.19$ and $C_{1j} = 7.8 \times 10^{-4}$.

The ratio of the N-year worst-month percentage exceedance X_{hj}. to Y_j, the average annual percentage exceedance for the same threshold j, is given by

$$Q_{jN} = \frac{X_{hj}}{Y_j} = \frac{\ln(12\,N\,C_{oj})}{C_{oj}} \tag{6.3-24}$$

For the case of N=1 year, this is bounded by:

$$\frac{12}{M} \leq Q_{j1} \leq 12 \tag{6.3-24}$$

Where M is the number of months in the year that intense rains typically fall. If $M < 3$, the exponential model should be questioned. The lower bound has been shown to be a fair estimate of Q_{j1} for rain rates with annual percentage exceedances in the .001% to .01% range.

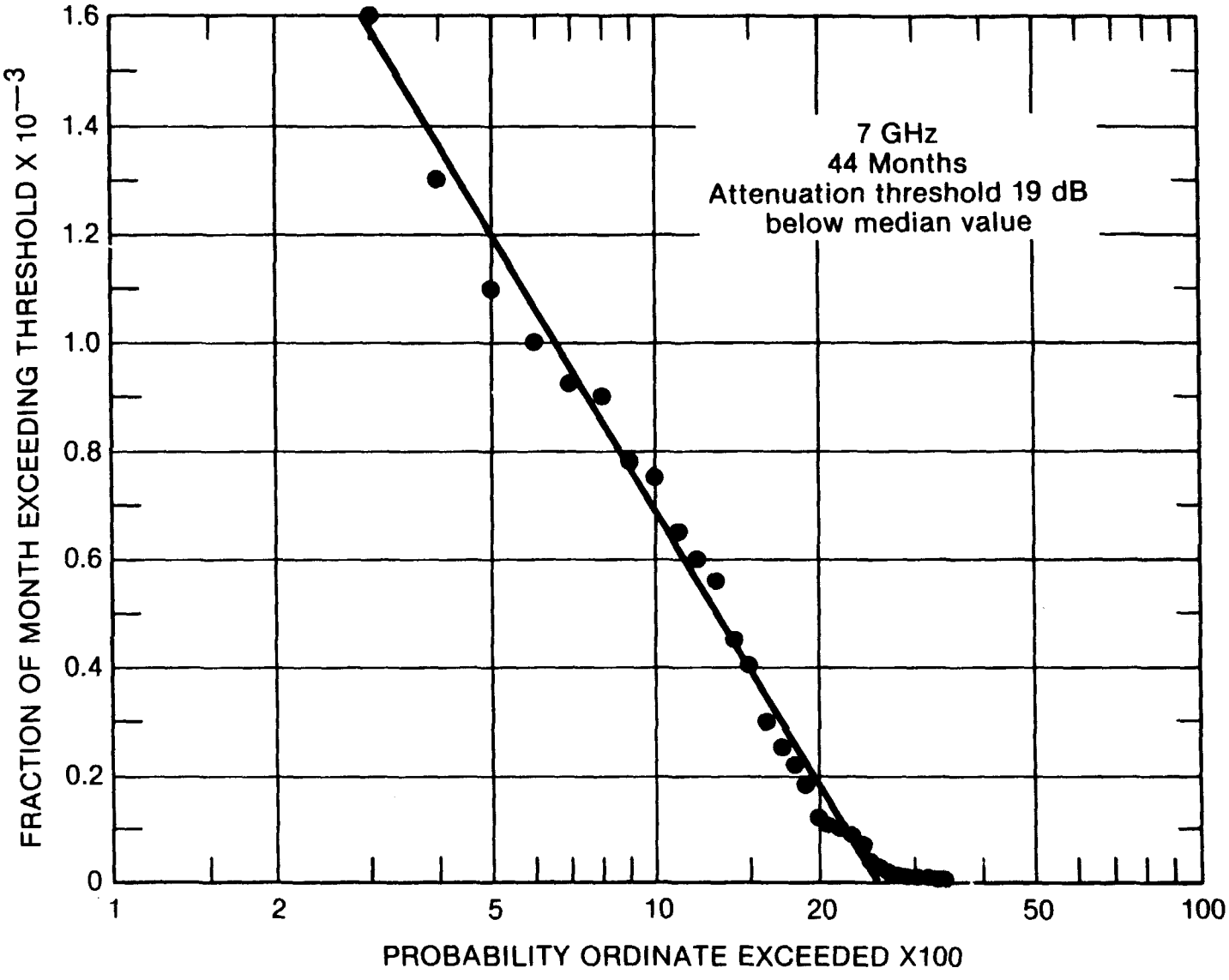

Figure 6.3-18. Probability of Attenuation Threshold Being Exceeded for the Indicated Fraction of Time Per Month (CCIR-1978, Rpt 723)

The worst-month versus annual probability relationship has been found to be closely approximated by a power law of the form

$$\overline{Q} = A\overline{Y}^{-\beta} \qquad (6.3\text{-}25)$$

where Q is the ratio of the average worst-month probability to the average annual probability (Y) and A and β are coefficients. The observed ranges of coefficient values are $1.2 \leq A \leq 3.3$ and $0.167 \leq \beta, \leq 0.074$ (CCIR Rep. 723-1, 1982a). A useful approximate relationship between worst-month exceedance time percentages (p) and annual time percentages (p_w) is (CCIR, 1982a):

$$p = 0.29\ p_w^{\ 1.15} \qquad (6.3\text{-}26)$$

where p and p_w are in percent. The corresponding coefficient values for the previous power law relationship are A = 1.64 and β = 0.13. These values yielded Q ratios in good agreement with average values for different locations in North America and Europe. For current CCIR recommendations, the reader is referred to CCIR report 723-2, "Worst Month Statistics", (CCIR, 1986e).

6.4 CLOUD, FOG, SAND AND DUST ATTENUATION

6.4.1 Specific Attenuation of Water Droplets

The water droplets that constitute clouds and fog are generally smaller than about .01 cm in diameter. This allows the Rayleigh approximation to be used to calculate specific attenuation in clouds and fog for frequencies up to 100 GHz. Using this approximation, the specific attenuation α_c is, unlike the case of rain, independent of the droplet size distribution. It is proportional to the liquid water content ρ_ℓ:

$$\alpha_c = K_c \rho_\ell \text{ dB/km} \qquad (6.4\text{-}1)$$

ρ_ℓ is normally expressed in units of g/m^3. The attenuation constant K_c is a function of frequency and temperature and is given by Figure 6.4.1 (CCIR Rpt. 721-1, 1982a). The curves given in the figure assume pure water droplets. The values for salt-water droplets, corresponding to ocean fogs and mists, are higher by approximately 25% at 20°C and 5% at 0°C (Koester and Kosowsky-1978).

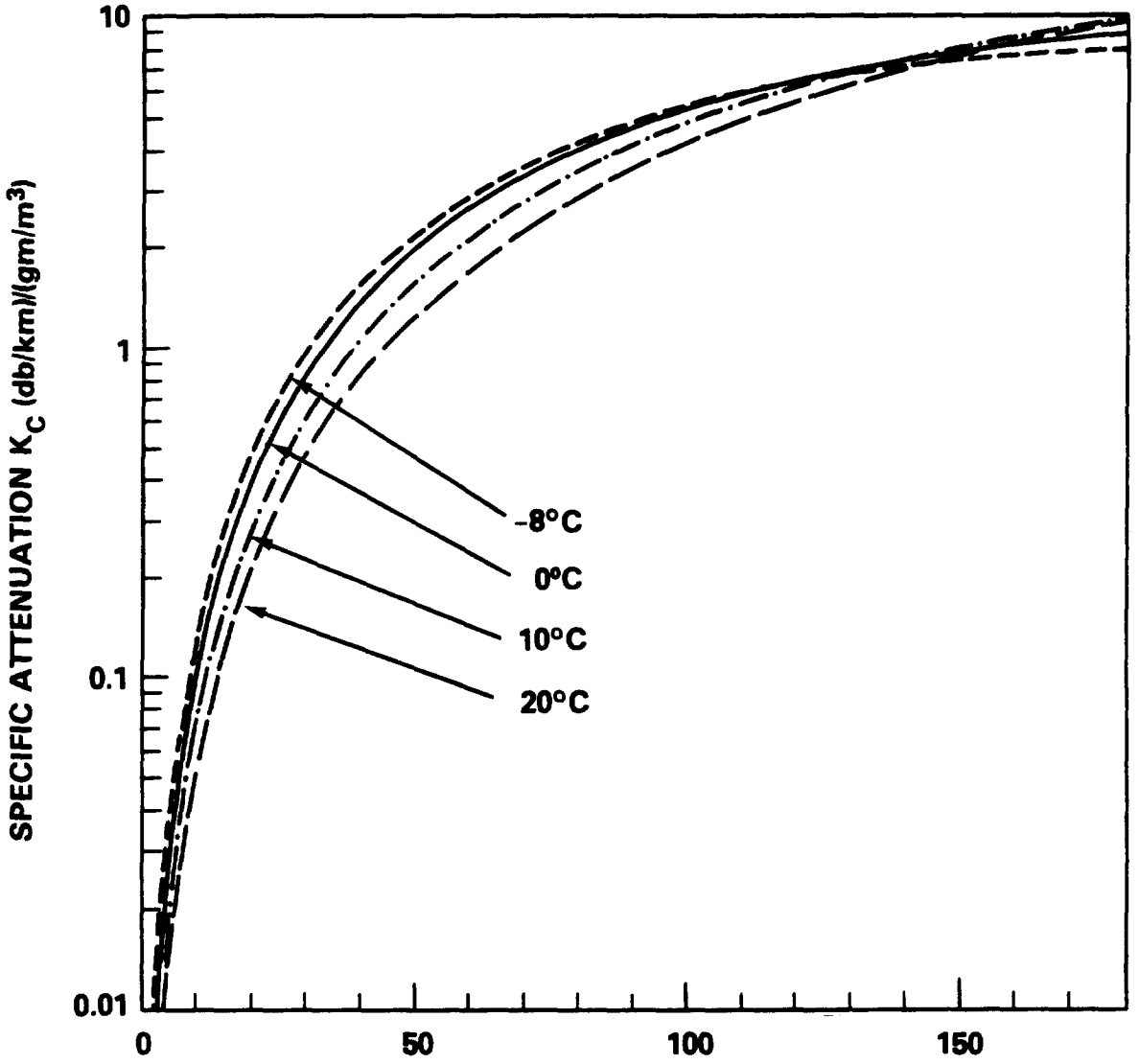

Figure 6.4-1. Attenuation Coefficient K_c Due to Water Droplets (from CCIR 1982a, Rpt 721-1)

6.4.2 Clouds

6.4.2.1 Water Content of Clouds. The liquid water content of clouds varies widely. For stratiform, or layered, clouds, the value was observed to most often fall in the range of 0.05 to 0.25 g/m^3. For the most dense of this type of cloud, stratocumulus, maximum values from 0.3 to 1.3 g/m^3 have been measured (Mason-1971). Cumulus clouds, especially the large cumulonimbus and cumulus congestus that accompany thunderstorms, have the highest values of liquid water content. Fair weather cumulus were found to have liquid water contents generally less than 1 g/m^3. Peak values exceeding 5 g/m were found in cumulus congestus clouds by Weickmann and aufm Kampe (1953). They estimated an average value of 2 g/m^3 for cumulus congestus and 2.5 g/m^3 for cumulonimbus. A review of typical values is given in Slobin (1982).

Clouds are not homogeneous masses of air containing evenly distributed droplets of water. Rather, the liquid water content can vary widely with location within a single cloud. On the average, the liquid water content in smaller cumulus congestus clouds increases fairly steadily with distance up from the base, then begins to drop off somewhere in the mid-to-upper parts. It also generally decreases with horizontal distance from the center toward the edges. Small-scale variations are also present, however. Sharp differences have been observed in localized regions on the order of 100 m across. One would expect fairly rapid local variation with time as well, due to the complex patterns of air movement taking place within cumulus clouds. Updraft wind velocities greater than 10 m/s exist within cumulonimbus clouds (Rogers-1976).

6.4.2.2 Measured Attenuation of Clouds. Typical path lengths through cumulus congestus clouds probably fall between about 2 and 8 km. Using the estimated average liquid water content from above (2 g/m^3), and the attenuation coefficient from Figure 6.4.1, this implies an added path loss at 35 GHz of about 4 to 16 dB. Fortunately, this calculation grossly overestimates the actual attenuation that has been observed through these clouds. This

appears to be generally true, as seen in Tables 6.4-1 and 6.4-2, which present measurements from two sources.

Table 6.4-1. Zenith Cloud Attenuation Measurements, From Lo, Fannin and Straiton (1975)

Cloud Type	Number of Observations	Mean Cloud Attenuation (dB)		Mean Gaseous Attenuation (dB)	
		35 GHz	95 GHz	35 GHz	95 GHz
Altocumulus	7	.02	.23	.38	1.93
Altostratus	2	.15	.30	.34	1.73
Stratocumulus	22	.18	.61	.43	2.14
Stratus	8	.13	.12	.42	2.14
Nimbostratus	5	.14	.11	.44	2.32
Cumulus	20	.12	.34	.41	2.12
Cumulonimbus	6	.34	2.36	.40	2.07

Table 6.4-2. Zenith Cloud Attenuation Measurements, CCIR Rpt. 721-2 (1986f)

Cloud Type	Cloud Attenuation (dB)	
	95 GHz	150 GHz
Stratocumulus	0.5 - 1	0.5 - 1
Small, Fine Weather Cumulus	0.5	0.5
Large Cumulus	1.5	2
Cumulonimbus	2 - 7	3 - 8
Nimbostratus (Rain Cloud)	2 - 4	5 - 7

In Table 6.4-1, the gaseous attenuation, calculated for the measured surface relative humidity, is given for comparison. The cloud attenuation is in most cases 40% or less of the gaseous attenuation. For frequencies removed from the 35 and 95 GHz "windows," the cloud attenuation would be a smaller fraction of gaseous attenuation. In Table 6.4-1, the number of observations is rather small for all but two types of clouds. The numbers given should therefore not be given undue statistical significance. Also, in using both tables, one should bear in mind the great variability in size and state of development of the clouds observed.

The 35 and 95 GHz data of Table 6.4-1 or 6.4-2 may be roughly scaled in frequency, using the frequency dependence of attenuation coefficient from Figure 6.4-1. Scaling in this manner is quite approximate, as is seen from Table 6.4-1. The ratio of attenuation coefficients at 35 and 95 GHz varies between about 3.9 for -8°C to 6.3 for 20°C. The ratio of average cloud attenuations measured at those frequencies is, from the table, 3.4 for stratocumulus, 2.8 for cumulus, and 6.9 for cumulonimbus. In another series of measurements on individual fair weather cumulus clouds (Lo, et al-1975) this ratio was usually between 3.7 and 5.5.

There appears to be a large discrepancy between tables 6.4-1 and 6.4-2 in the attenuation of nimbostratus clouds at 95 GHz. The large values of Table 6.4-2 may be due to the inclusion of precipitation in the path, however, because the presence of nimbostratus clouds would usually be accompanied, sooner or later, by precipitation at the ground station, the higher values of attenuation would be expected. This does not necessarily apply to cumulonimbus clouds, however. Because of the large vertical development and limited horizontal extent of these clouds, a typical (30-40° elevation angle) propagation path may be intercepted by them without significant rainfall at the ground station.

6.4.2.3 Statistics of Microwave Effects of Clouds. A JPL study (Slobin 1982), has made estimates of the statistics of cloud effects for the continental U.S., Alaska and Hawaii. The presence of clouds in space-earth downlink antenna beams has two primary effects: signal attenuation, and an increase in system noise temperature. For very low-noise receiving systems, such as those used for deep-space communications, the noise effect can be quite significant. Cloud noise statistics may therefore be important in siting such systems and in scheduling their use. Cloud effects can normally be ignored in a high-reliability system designed with a rain margin. However, clouds must be considered for systems with minimal margin that are intended for continuous use, such as a deep-space link receiving unrepeatable spacecraft data.

The JPL study determined that the U.S. could be divided into fifteen regions of statistically "consistent" clouds, as shown in Figure 6.4-2. The region boundaries shown in the figure are highly stylized and should be interpreted liberally. Some boundaries coincide with major mountain ranges (Cascades, Rockies, and Sierra Nevada), and similarities may be noted between the cloud regions and the rain rate regions of the Global Model. Each cloud region is considered to be characterized by observations at a particular National Weather Service observation station. The locations and three-letter identifiers of these stations are shown in the figure. For each of these stations, an "average year" was selected on the basis of rainfall measurements. The "average year" was taken to be the one in which the year's monthly rainfall distribution best matched the 30-year average monthly distribution. Hourly surface observations for the "average year" for each station were used to derive cumulative distributions of zenith attenuation and noise temperature due to oxygen, water vapor, and clouds, for a number of frequencies ranging from 8.5 to 90 GHz.

The following method was employed to calculate the cumulative distributions.

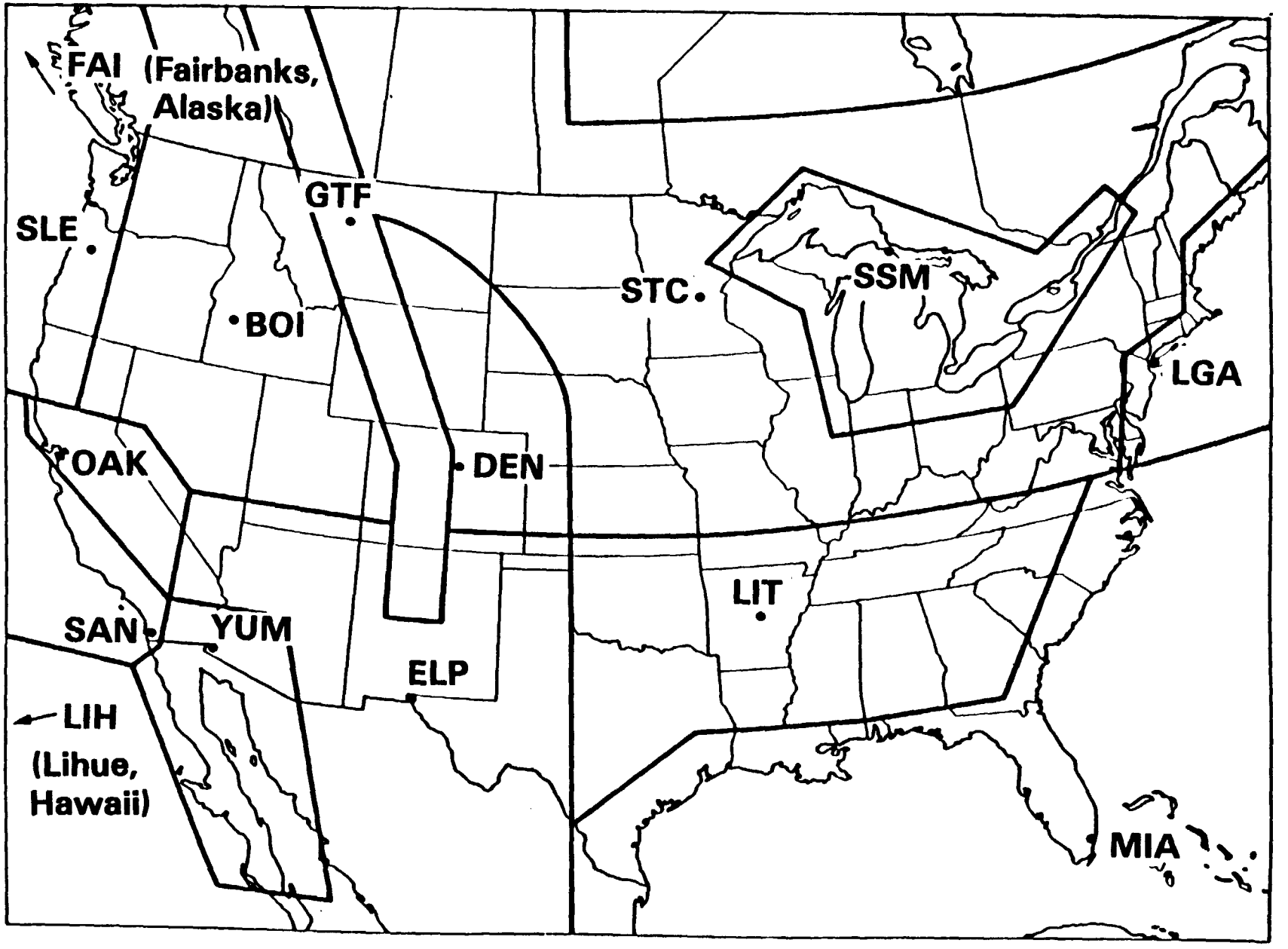

Figure 6.4-2. Consistent Cloud Regions

- For each hour's observations, the attenuation of each reported cloud layer (up to four) was calculated based on the layer's water particle density, thickness, and temperature. The attenuation due to water vapor and oxygen was also found using the reported surface conditions.

- Total attenuation and noise temperature due to all cloud layers and gases were calculated for sixteen possible cloud configurations, corresponding to all combinations of cloud presence or absence at the four layer heights.

- Cumulative probability distributions for attenuation and noise temperature were calculated using the reported percent-coverage values corresponding to each cloud layer. For example, if the percentage of coverage was 60 percent for layer 1 and 20 percent for layer 2, then the probability of various configurations of clouds present in the antenna beam would be as follows:

no clouds present:	(1-.6) (1-.2) = 0.32
layer 1 clouds only present:	(.6) (1-.2) = 0.48
layer 2 clouds only present:	(1-.6) (.2) = 0.08
clouds in both layers present:	(.6) (.2) = 0.12

Typical cumulative attenuation and noise temperature distributions calculated in this way are shown in Figure 6.4-3. The curves apply to zenith paths only, but can be extended to slant paths using a cosecant law. Such extension will probably lead to overestimation at low elevation angles and small time percentages. This is because clouds with large vertical development have less thickness for slant paths than for zenith paths. At time percentages where rain effects become significant (cumulative distributions greater than 95%), the attenuation and noise temperature due to the rain should be considered also.